The contribution of hydrogen peroxide to the radiosensitizing effect of gold nanoparticles

Talat Tariq Khalil, Rana Bazzi, Stéphane Roux, Michel Fromm

The contribution of hydrogen peroxide to the radiosensitizing effect of gold nanoparticles

Talat Tariq Khalil[a,c], Rana Bazzi[b], Stéphane Roux[b], Michel Fromm*[a]

[a] Université de Bourgogne Franche-Comté, UMR CNRS 6249 Chrono-Environnement, 16 route de Gray, 25030 Besançon Cedex, France.

[b] Université de Bourgogne Franche-Comté, UMR CNRS 6213 Institut UTINAM, 16 route de Gray, 25030 Besançon Cedex, France.

[c] Chemistry department, college of women science, Babylon University, PO Box: 4 Iraq - Babylon - Hilla

Corresponding Author: Michel Fromm, michel.fromm@univ-fcomte.fr, Tel: (0) 33 381 666 560, Fax: (0) 33 381 666 522

Keywords: *Gold nanoparticles, ROS scavenger, Hydrogen peroxide, Ultra-soft X-rays, Plasmid DNA*

Abstract:

Plasmid DNA in aerated aqueous solution is used as a probe to determine whose of the reactive oxygen species (ROS) generated after absorption of ultra-soft X-rays (USX) take part in biomolecule damage in the presence and in absence of Gold Nano-Particles (GNP) and specific scavengers. Citrate-coated GNPs with core sizes of 6, 10 and 25 nm are synthetized and characterized, especially in terms of plasmon band shift, ζ-potential and hydrodynamic radii (respectively 9, 21 and 30 nm). We confirm the radiosensitizing effect of GNP and show that the SSB number per plasmid increases when, for a same mass of gold element, the core size of the gold nanoparticles decreases. Hydroxyl radicals ($^{\bullet}OH$) are scavenged using the positively-charged 2-amino-2-hydroxymethyl-1,3-propanediol (TRIS) and the neutral dimethyl sulfoxide (DMSO) molecules. Due to both negatively-charged environments of DNA and GNP, at identical scavenging capacity, TRIS is more effective at quenching $^{\bullet}OH$ than DMSO. The strong radiosensitizing effect of hydroxyl radicals is confirmed. Methanoate anions are then used to transform $^{\bullet}OH$ into hydrogen peroxide; the latter being known to be non-aggressive regarding DNA in the absence of easily oxidable metallic ions (Fenton reactions). Surprisingly, in the presence of GNP, high DNA damage yields are observed even though hydrogen peroxide might not be hold as responsible. Conversely, the radiosensitizing effect of GNP is not observed anymore when H_2O_2 is scavenged using pyruvate ions. We demonstrate that hydrogen peroxide constitutes quite unexpectedly a hidden stock of $^{\bullet}OH$ which are activated at the surface of the GNP by decomposition of H_2O_2 molecules.

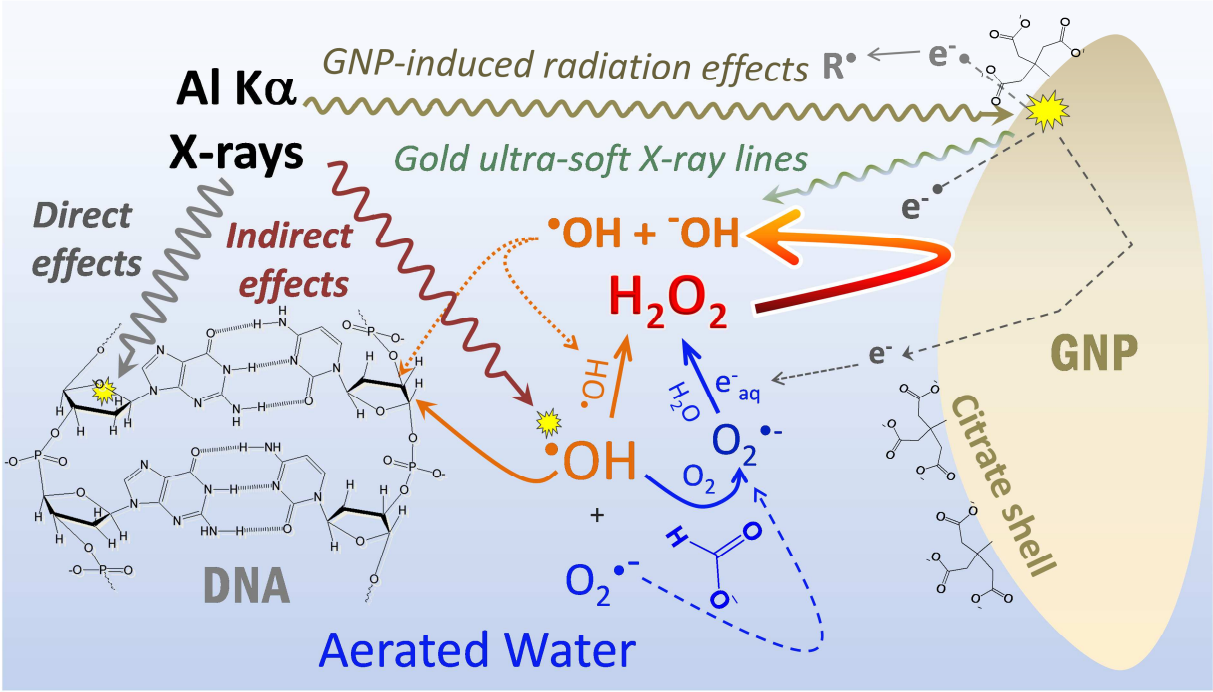

Highlights

• Plasmid DNA used as a probe in presence and absence of GNPs during X-ray irradiation

• At constant mass of gold, the damages increase as the GNP core size decreases

• Ultra-soft X-rays favor OH radical recombination during water radiolysis

• The use of specific scavengers allows demonstrating the damaging activity of H2O2

• The damaging activity is confirmed by H2O2 addition

I. Introduction

The radiotherapy is, alone or in combination with surgery and/or chemotherapy, commonly used for treating malignant solid tumors [1]. This strategy rests on the exposure of the tumor zone to ionizing radiation. The absorption of ionizing radiation by the various cell components induces a cascade of physical, chemical and biological reactions which lead under optimal conditions, to the eradication of the cells [2]. Since the chemical composition of cancerous and normal cells is very similar, there is almost no difference in the absorption between cancerous and normal cells. The low selectivity of the radiotherapy is reflected by the undesirable alteration of surrounding healthy tissues which constitutes the major weakness of this cancer therapy. In order to overcome the lack of selectivity of the radiotherapy, the use of radiosensitizing agents (or radiosensitizers) was proposed [3], [4]. Owing to the high atomic number (Z) of their components, the radiosensitizers exhibit a great propensity to absorb the ionizing radiation. In other words, their presence in the tumor is expected to induce higher damage because energy absorption may generate a highly localized radiation dose within the tumor. This implies that the radiosensitizers are preferentially located into the tumor. For this reason, nanoparticles appear more suited than molecules. The nanoparticles exhibit indeed a more controlled biodistribution and a greater amount of high Z elements (up to 10^5 *vs* <10 for molecules) [5], [6], [7]. Moreover one of the main characteristics of the nanoparticles rests on the possibility to gather in a reduced volume a large range of complementary properties which can be exploited for combining imaging and therapy [8], [9], [10], [11], [12] [13]. Among the multifunctional radiosensitizing nanoparticles, gold and platinum nanoparticles and nanostructures combining gold and platinum are probably the most studied and the most promising.

The radiosensitizing effect of gold particles was first described by Herold *et al*. [14] but the particles synthesized for this experiment were too large (1.5-3 µm) for a clinical application

even for an intratumoral injection. Although nanoparticles are quickly removed from body by renal clearance, Hainfeld *et al.* [15] demonstrated that mammary tumor-bearing mice benefit from a great increase in lifespan when they are treated by radiotherapy (250 kVp X-rays) after intravenous injection of 1.9 nm sized-gold nanoparticles. The efficiency of gold nanoparticles for improving the effect of the radiotherapy relies in the *in vivo* behavior of these nanoparticles (renal clearance, absence of undesirable accumulation in healthy tissue, preferential accumulation in tumor by enhanced permeability and retention (EPR)) effect but also on their peculiar interaction with the ionizing radiation [11], [15], [16]. Butterworth and his colleagues demonstrated indeed that gold nanoparticles (core size ~2 nm) are the most suited for generating high damage to biological media [17], [18]. Although the propensity to absorb X-ray photons does not depend on the size of the gold core, the release of electrons (ionization of gold element) is more important in the case of the gold nanoparticles because the probability to be entrapped in the gold core is lower in the smallest nanoparticles [17], [18]. Their association with water (the main component of biological medium), oxygen but also with biomolecules (proteins, lipids, nucleic acids) provide highly reactive species (*e.g.* reactive oxygen, ROS) which can induce cell death because of serious alterations of their structure and functions [17], [19]. Many studies have been performed for determining the mechanisms of the radiosensitization in presence of gold nanoparticles [20], [21]. Unfortunately, the experimental conditions are so different that it is not easy to compare and therefore conclude. However, it appears that essentially hydroxyl radicals are suspected to play significant role in cellular alteration after exposure to ionizing radiation in presence of gold nanoparticles [21], [22]. More generally nevertheless, elevated ROS production is considered as part of GNP radiosensitization [19], [20]. In order to clarify the role of each active species, we envisage to scavenge separately each of the formed ROS with or without gold nanoparticles and, at the same time, to use plasmid DNA as a probe for quantifying DNA

damages. To be clear, we do not hypothesize on the fact that in real biological situation GNPs are localized in the cell nucleus or whether they "directly" damage DNA or not; here DNA is actually used only as a probe which permits to easily evaluate the physical and chemical behavior of GNPs after exposition to ionizing radiations in various chemical environments. The data collected from these experiments would provide relevant information for explaining the enhancement of the dose effect when irradiation is performed in presence of GNPs.

The present work is guided by two main observations. Firstly, calculations realized in the field of Au/TiO_2 catalysts have shown that hydrogen peroxide undergoes facile HO–OH cleavage on Au metal clusters without a barrier to form hydroxyl groups [23]. Such a process was experimentally observed when gold nanoparticles supported on Fenton treated diamond nanoparticles (Au/DNP) where found to be a highly efficient catalyst to promote the generation of hydroxyl radicals from H_2O_2 [24].

Secondly, the extent of the reactions that contribute to the decay of $^{\bullet}OH$ all have a pronounced maximum (in absolute value) of ~1 keV, which means that there are less $^{\bullet}OH$ surviving spur reactions at this energy (*i.e.* more recombination reactions). It should be remembered that a spur is a small domain of the radiation track; it is defined so that less than 100 eV were deposited within such a local volume [25], [26], [27]. Al K_α ultra-soft X-rays (USX) of 1.5 keV will thus be used in this study as they are a very effective source for the local production (at the nanometer scale) of large amounts of $^{\bullet}OH$ radicals in aqueous solution, those latter radicals being likely to recombine thus forming H_2O_2. H_2O_2 has no direct damaging effect on DNA but it is known that if oxidizable metallic atoms are present a Fenton-like mechanism occurs [28], H_2O_2 will therefore also be examined (scavenged) in this study [28].

II. Materials and methods

DNA samples and chemicals

Plasmid DNA (pUC21, 3266 bp) with initial concentration of 1000 ng/µL in ultra-pure water was purchased from PlasmidFactory GmbH & Co. KG (Germany). Supercoiled state measured by gel electrophoresis is predominant (>95%). The stock solution was stored at –80°C, and the plasmid pUC21 concentration was determined by measuring the absorbance at 260 nm, taking molar absorption coefficient to be = 5.3 x 10^7 cm^{-1} M^{-1} [29]. TRIS, DMSO, Methanoate and Pyruvate scavengers were purchased from Sigma-Aldrich Chemie S.A.R.L. (France).

GNP synthesis

The synthesis of gold nanoparticles was carried out in glassware which was treated prior to the reaction by aqua regia (two portions of hydrochloric acid (37%) and one portion of nitric acid (64%)), thoroughly rinsed with distilled water in order to dissolve any nucleation site. The compounds were purchased from Sigma Aldrich.

The colloidal GNP of 10 nm and 25 nm diameter were prepared according to the protocol of Turkevich-Frens [30]. The synthesis was based on the reduction of a gold salt ($HAuCl_4$.3 H_2O) by sodium citrate in the aqueous phase. Citrate acts as protective agent, so this method does not need the use of any other stabilizer. An aqueous solution of $HAuCl_4$ (30 mL, 0.01%by mass) was introduced in a 100 mL flask equipped with a condenser column and heated with vigorous stirring until boiling. Then, sodium citrate (38.8 mM, 600 µL (10 nm) and 450 µL (25 nm)) was added to this boiling solution for the synthesis of gold nanoparticles with core size of 10 nm and 25 nm, respectively. Once cooled to room temperature, the solution was purified by centrifugation (5 min at 6,000 g). The colloids were stored at 4 °C in darkness.

The smallest GNP of the series (core size: 6 nm) were obtained by the reduction of gold salt ($HAuCl_4$.3 H_2O) using a stronger reducing agent ($NaBH_4$) in presence of sodium citrate as stabilizer. An aqueous solution of gold salt (10 mg in 1 mL of ultrapure water) was poured

with 90 mL of water under magnetic stirring. After 1 minute at room temperature, an aqueous solution of sodium citrate (2 mL, 38.8 mM) was mixed with the gold salt solution while stirring. A freshly prepared $NaBH_4$ aqueous solution (1 mL, 0.075% by mass) was added to the solution containing the gold salt and sodium citrate. The resulting mixture was stirred for 5 minutes and then stored at 4 ° C in darkness.

Gold nanoparticles characterization

UV-Visible spectroscopy

Absorption spectra of gold nanoparticle colloids were recorded in the visible domain of the electromagnetic spectrum (400 - 800 nm) using a UV-visible spectrophotometer (Varian, Cary 100 Scan). Aqueous suspensions ([Au] = 0.5 mM) were put in quartz reservoirs of 1cm optical path length.

Dynamic light scattering (DLS) and zeta potential measurements

Direct determination of the hydrodynamic diameter and zeta potential (ζ-potential) of GNP was performed at pH 7.4 with a Nanosizer ZS from Malvern Instrument comprising a He-Ne laser (wavelength: 633 nm).

Transmission electron microscopy (TEM)

TEM was performed to obtain detailed morphological information about the samples and to measure the size of the gold cores (from the analysis of at least 100 nanoparticles on several micrographs for each sample). TEM was carried out using a JEOL 2010 microscope operating at 200 kV (Laboratoire Interdisciplinaire Carnot de Bourgogne, Dijon, France). The samples for TEM were prepared by depositing a drop of a diluted colloidal solution on a carbon grid and allowing the liquid to dry in air at room temperature.

X-ray irradiation

The irradiation technique was described in details elsewhere [31]. Briefly described, the aqueous solution has a 2 mm thickness and 8 mm diameter (total volume of 100 µL), the irradiation was generated with a cold cathode source (1.5 keV, Al Kα). The irradiation of DNA was performed at controlled constant room temperature (295 K) and at constant 98% RH (humidity) [31]. Irradiation of 100 µL of plasmid aqueous solution was performed using a cylindrical 8 mm-diameter sample holder under constant stirring rate of 110 RPM. Due to the short attenuation length of Al Kα photons in water, stirring at 110 RPM was demonstrated to be mandatory for an homogeneous dose deposited in the liquid sample [31]. The absorbed dose rate (determined using Fricke dosimetry) is constant and equal to 2.23 $Gy.min^{-1}$ [31]; all series of samples were exposed to USX for 0, 5, 10, 15, 20, 30, 40 minutes (i.e. 0, 11, 22, 34, 45, 67, 89 Gy). Measured DNA damage yields (single strand breaks per plasmid) are linear functions when plotted versus dose within a given series of experiments, which enables the rates expressed in single strand $break.plasmid^{-1}.Gy^{-1}$ to be determined.

DNA was diluted to reach target concentration (final concentration of 4.69 nM) in absence and in presence of GNP (up to 46.9 nM, *i.e.* 10 GNP per DNA plasmid). In the case of GNP with a core size of 10 nm (46.9 nM, 10 GNP per DNA), irradiation was also carried out with various concentrations of specific scavengers (TRIS, DMSO, Methanoate, Pyruvate).

Agarose gel electrophoresis and strand break determination

Immediately after irradiation, an equivalent of 100 ng of DNA from each sample was loaded per well of agarose gel and electrophoresed. The supercoiled (S), relaxed (or circular; C) and linear form (L) band smears are imaged and quantified by fluorescence of the gel at 302 nm using the DocTM XR system (BioRad) and Quantity One (BioRad) software. Reagents for gel electrophoresis were purchased from Life Technologies SAS (France); namely UltraPure DNA Typing Grade 50X TAE buffer, 10×Bluejuice gel loading buffer, and SYBR Safe DNA

gel stain. Statistical treatment allowed the determination of average numbers of SSB per plasmid using the following relationships:

$$SSB = \ln[(1-L)/S] \quad (1)$$

where S and L are the fraction of detectable molecules corresponding to supercoiled and linear forms of DNA plasmid [32]. Supercoiled (S), Relaxed or Circular (C) and linear (L) forms of plasmid DNA are topological states of covalently closed circular (ccc) double stranded DNA (plasmid DNA). The S state corresponds to the native state (without nicking), typically > 95% in our case. C form is the resulting state after one nick (i.e. one strand break), L is the result of two nicks separated by less than 10 base pairs within the same plasmid; thus leading to the complete break of opposite strands in DNA; called double strand break (DSB). Such topologies are easily quantified (separated) using Agarose Gel Electrophoresis. Single-strand breaks (SSBs) were used to quantify the dose enhancement at the addition of GNPs.

III. Results and Discussion

Gold nanoparticles

Irradiation experiments were carried out with citrate coated gold nanoparticles with three different core sizes (6, 10 and 25 nm). Dimensions were determined using TEM images analyses (Fig. 1).

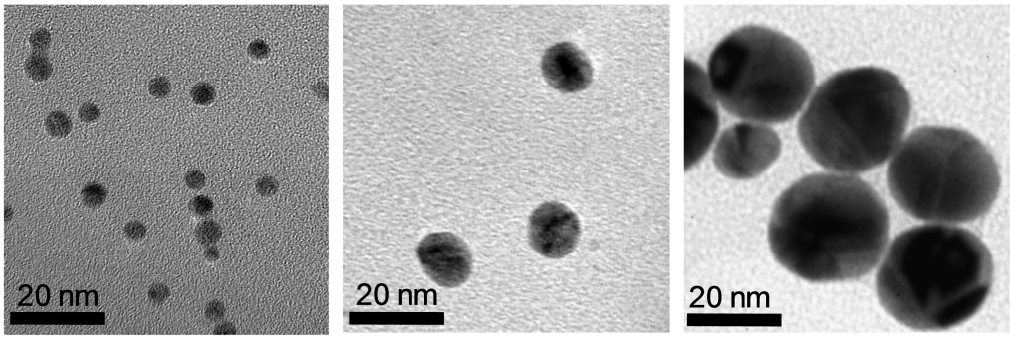

Fig. 1. *TEM micrograph of citrate-coated gold nanoparticles with a core size of 6, 10 and 25 nm (from left to right).*

The 10 and 25 nm sized nanoparticles were prepared according to the Turkevich-Frens [30] protocol while the smallest ones (6 nm) were prepared by using a stronger reducing agent (sodium borohydride instead of sodium citrate) in presence of citrate anions. The two different sizes (10 and 25 nm) were obtained by varying the amount of citrate anions for a fixed amount of gold salt. The increase of the molar citrate-to-gold salt ratio is reflected by a decrease of the size. The replacement of citrate anions by borohydride anions as reducing species led also to the reduction of the core size [33]. However this strategy requires the use of stabilizing molecules for controlling the growth of the nanoparticles and for avoiding the agglomeration because in contrast to citrate anions, $NaBH_4$ is unable to behave as a stabilizer. In order to have the same organic shell for the three different samples, the reduction of the gold salt by sodium borohydride was carried out in presence of citrate anions. Besides the data retrieved from TEM experiments, the difference in the core size was confirmed by UV spectra since the plasmon band of the gold suspensions is shifted to the red (*i.e.* the high wavelengths) when the core size increases [34] (Table 1).

Such a shift is illustrated by the color change of the colloid from the orange (for the smallest nanoparticles) to intense red (for the largest ones). This increase in size is also revealed by the measurement of hydrodynamic diameter (D_h) which is based on Dynamic Light Scattering or DLS (Table 1). It must be pointed out that hydrodynamic diameter is larger than the core size since, in addition to the size of the core, the D_h value takes into account the thickness of the organic shell and of the adsorbed solvent layer. Indirectly, the DLS experiments confirm the presence of an organic shell onto the gold core. The presence of citrate anions onto the gold core is suspected since the sign of the zeta-potential which reflects the outer charge of the particles is negative (Table 1).

	Au@citrate (6 nm)	Au@citrate (10 nm)	Au@citrate (25 nm)
∅ (nm)	6.1 ± 0.5	12.2 ± 1.0	24.2 ± 2.5
D_h (nm)	8.9 ± 0.4	21.1 ± 0.5	30.2 ± 3.0
ζ-potential (mV)	-47.5	-30.8	-31.0
λ_{max} (nm)	519	521	525

Table 1. Main characteristics of GNP (core diameter (∅), hydrodynamic diameter (D_h), ζ-potential at pH 7.4, wavelength at the maximum of the plasmon band (λ_{max}))

The ROS and their scavengers

The irradiation of water by ultrasoft X-ray beam (1.5 keV) yields mainly $^{\bullet}OH$, $H^{\bullet}$ and e^-_{aq}. These reactive species exhibit a great potential for altering biomolecules and therefore the functions of cells. However their potential can be reduced by concurrent reactions. Combination of $^{\bullet}OH$ radicals provides hydrogen peroxide (H_2O_2) which is less aggressive than $^{\bullet}OH$. In the case of aerated solutions, $H^{\bullet}$ and e^-_{aq} reacts with oxygen (O_2). Their reaction leads to the formation of hydroperoxide ($HO_2^{\bullet}$) radical and superoxide anion radical ($O_2^{\bullet-}$) which finally provide after multistep recombination molecular hydrogen (H_2) and H_2O_2. Radiolytic yields and reaction pathways are provided using the data published by Yamaguchi and collaborators [35].

Radiolysis of water by ultrasoft X-ray beam.

When exposed to radiation, water undergoes a breakdown sequence into hydroxyl radical, hydrogen radical and hydrated electron. If 1.5 keV photons are used, radiolytic yields (for 100 eV of absorbed energy) at one nanosecond are respectively 3.2, 1.2 and 2.6. The three primary radiolytic products recombine to produce H_2, H_2O and H^+ [31], [35]. In the present case of aerated water (presence of molecular oxygen), hydrogen radicals and hydrated electrons quickly react with molecular oxygen and the final products are $^{\bullet}OH$ (hydroxyl radical) and $HO^{\bullet}_2/O_2^{\bullet-}$ (the peroxide radical in equilibrium with the superoxide anion) with

respective radiolytic yields at one nanosecond 3.2 and 3.8 for 100 eV of absorbed energy. These unstable species can rapidly recombine to produce H_2 and H_2O_2 [31], [35]. Due to both its high radiolytic yield and extremely high reactivity (damaging potential), the hydroxyl radical is generally considered in radiation biology as the main damaging species, [35]. In order to evaluate the role of the different ROS, specific scavengers were used. TRIS (equation (2)) and DMSO (equation (3)) were chosen for their ability to scavenge the oxygen centered •OH radicals which are recognized to play an important role in the alteration of cells [36]. Hydroxyl radicals are scavenged by TRIS and DMSO with extremely high kinetic rate constants, k_{TRIS}= 1.5 x 10^9 L.mol^{-1}. s^{-1} and k_{DMSO} = 7 x 10^9 L.mol^{-1}. s^{-1}[37], [38].

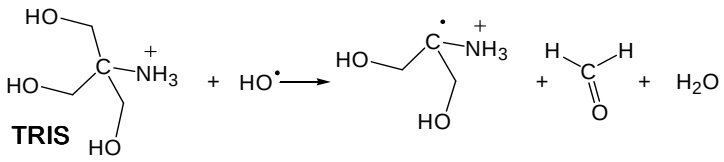

(2)

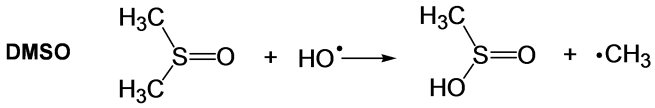

(3)

Another way to counteract the effect of hydroxyl radicals is to transform them into hydrogen peroxide (via the formation of hydroperoxide radical and superoxide anion radical), *i.e.* thus forming less reactive species. This conversion can be achieved by adding methanoate ions to the mixture (equations (4)) [39], [40]. Methanoate anions have the propensity to scavenge •OH radicals in such a way that in the presence of dissolved oxygen, superoxide anion radical temporarily are formed [41]. Those latter anions thus react extremely rapidly with aqueous or "dissolved" electrons finally providing hydrogen peroxide:

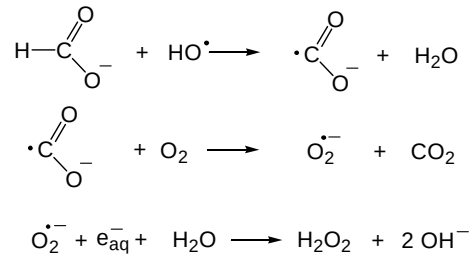

(4)

The respective pseudo-first order rate constants for these three reactions are k=3.5 x 10^9 L.mol^{-1}. s^{-1}, k=2.4 x 10^9 L.mol^{-1}. s^{-1} and k=1.3 x 10^{10} L.mol^{-1}. s^{-1} [41]. All three reactions are very fast reactions.

With the scavenging capacity σ (s^{-1}) defined as σ = k [scavenger], the lifetime of any species of known scavenging capacity (σ) is τ = 1/σ. That is to say that within a 100 mM scavenger concentration and a kinetic constant of the order of 10^9 L.mol^{-1}. s^{-1}, the average lifetime of $^{\bullet}$OH is reduced to only 10 ns. The mean diffusion distance of $^{\bullet}$OH radicals under given scavenging conditions can be calculated using; $\langle x \rangle = 2.26 (D\tau)^{1/2}$ [42]. With the diffusion coefficient of $^{\bullet}$OH radicals D = 2 x 10^{-5} cm^2 s^{-1} in water [43], the mean diffusion distance of these radicals is 10 nm if the scavenger rate constant is 10^9 L.mol^{-1}. s^{-1}. A 300 mM concentration of TRIS confines the average displacement of $^{\bullet}$OH radical within 4.8 nm (namely a shorter distance that the diameter of the smallest nanoparticles used in this study).

In order to evaluate its possible action, hydrogen peroxide was scavenged by pyruvate anions [44] (equation (5)).

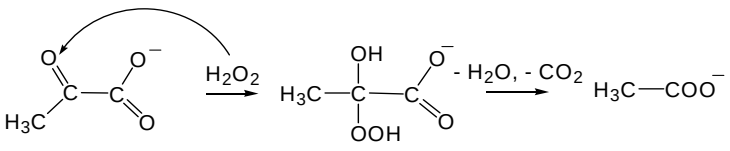

(5)

Hydrogen peroxide is the least reactive molecule among reactive oxygen species and is stable under physiological pH and temperature in the absence of metal ions [45]. It is regarded as being poorly reactive. Intracellular concentrations of pyruvate are of the order of 0.5 mM [46], and levels of 1.5 mM can be achieved in mitochondria [47]. Pyruvate *in vitro* is more efficient at scavenging H_2O_2 than GSH (GSH is for Glutathione ; the major cellular thiol

participating in cellular redox reactions, thus preventing damage to important cellular components caused by reactive oxygen species, peroxides, lipid peroxides, and heavy metals.) [48]. As an oxygen-centered non-radical, H_2O_2 is scavenged by pyruvate following a kinetic constant that varies from 0.75 to 2.2 $L.mol^{-1}. s^{-1}$, depending on the measurement method [44], [49].

The radiosensitizing effect of citrate coated-gold nanoparticles

In a preliminary step, the radiosensitizng effect of each type of gold nanoparticles was compared. Plasmid DNA in aqueous solution was exposed to ultrasoft X-ray beam with and without gold nanoparticles. The comparison between each case shows that the presence of gold nanoparticles (whatever the size) induces a greater amount of damage: the amount of single strand breaks (SSB) of plasmid DNA is lower when plasmids are irradiated without gold nanoparticles (Table 2 lines a0 and a1). This confirms the radiosensitizing effect of the citrate-coated gold nanoparticles. Interestingly, the SSB number per plasmid increases when, for a same mass of gold element, the core size of the gold nanoparticles decreases (Fig. 2). In other words, the radiosensitizing effect of gold atoms is more efficient when they are packed in the smallest nanoparticles. This observation is in line with the studies of Butterworth *et al.* [19].

For practical reasons, the determination of the role of the main ROS was performed with the intermediate size of gold nanoparticles (10 nm).

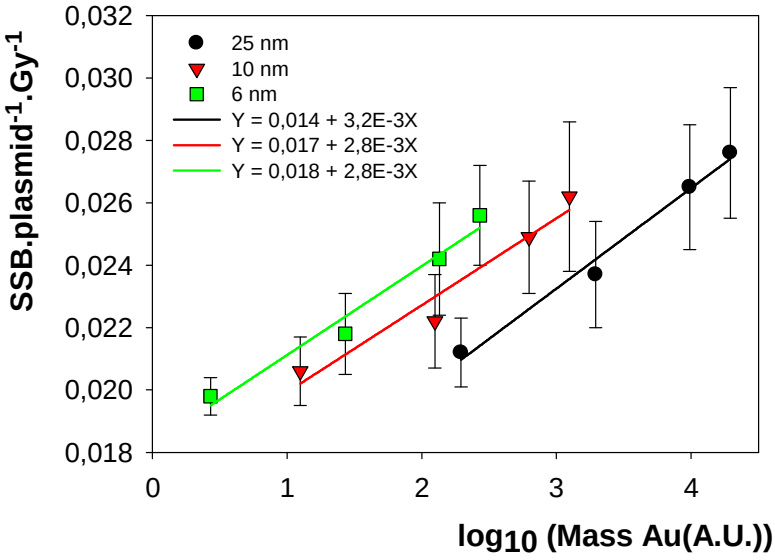

Fig. 2 *Influence of the size of the gold core on the SSB. Number of SSB per plasmid per Gray as a function of mass of gold in the suspension for different sizes of gold core. Error bars are the standard deviations stemming from a linear regression performed over 7 experimental points (SSB.plasmid^{-1} vs. dose).*

Whatever the experimental conditions, we can notice that the use of a scavenger induces a decrease of SSB yield (Fig. 3, Table 2). However differences exist between each scavenger used for this study. Since hydroxyl radicals produced by the radiolysis of water play an important role in the alteration of biomolecules and cells, a peculiar attention will be focused on the action of TRIS and DMSO which are well known specific $^{\bullet}OH$ quenchers. When irradiation is performed in presence of TRIS or DMSO, as expected SSB yields decrease while the concentration of scavengers increases (Fig. 3, Table 2 b0-b31 and c0-c11). Surprisingly, the scavenging effect (*i.e.* the decrease of SSB yield) is more important when TRIS is used whereas DMSO exhibits a higher scavenging capacity σ (s^{-1}) at the same concentration ($7x10^8$ s^{-1} vs $1.5x10^8$ s^{-1} at 100 mM).

	Experimental conditions DNA & GNP concentrations ($ng.\mu L^{-1}$)	Scavengers (mM)	SSB ± SD ($plasmid^{-1}.Gy^{-1}$)	$10^{-6}\times\sigma$ [a] (s^{-1})	SSB_{XAu}/SSB_X [b]
a0	pUC21 (10 $ng.\mu L^{-1}$)	/	0.0194±6.00E-04		
a1	[GNP] = 10 [pUC21]	/	0.0265±0.24E-04		1.37
b0	pUC21	1 mM Tris	0.0082±8.00E-04	1.5	
b1	[GNP] = 10 [pUC21]	1mM Tris	0.0116±5.00E-04	1.5	1.41
b10	pUC21	10 mM Tris	0.0022±1.00E-04	15	
b11	[GNP] = 10 [pUC21]	10 mM Tris	0.0029±2.00E-04	15	1.31
b20	pUC21	100 mM Tris	0.0010±1.00E-04	150	
b21	[GNP] = 10 [pUC21]	100 mM Tris	0.0011±1.00E-04	150	1.10
b30	pUC21	300 mM Tris	0.0007±1.00E-04	450	
b31	[GNP] = 10 [pUC21]	300 mM Tris	0.0007±1.00E-04	450	1.00
c0	pUC21 +	100 mM DMSO	0.0022±2.00E-04	700	
c1	[GNP] = 10 [pUC21]	100 mM DMSO	0.0027±2.00E-04	700	1.22
c10	pUC21	300 mM DMSO	0.0018±2.00E-04	2100	
c11	[GNP] = 10 [pUC21]	300 mM DMSO	0.0022±2.00E-04	2100	1.22
d0	pUC21	10mM methanoate	0.0054±4.00E-04	35	
d1	[GNP] = 10 [pUC21]	10mM methanoate	0.0124±4.00E-04	35	2.29
d10	pUC21	100mM methanoate	0.0051±3.00E-04	350	
d11	[GNP] = 10 [pUC21]	100mM methanoate	0.0119±5.00E-04	350	2.33
e0	pUC21	10mM pyruvate	0.0113±5.00E-04		
e1	[GNP] = 10 [pUC21]	10 mM pyruvate	0.0115±5.00E-04		1.02
e10	pUC21	100 mM pyruvate	0.0112±6.00E-04		
e11	[GNP] = 10 [pUC21]	100 mM pyruvate	0.0114±5.00E-04		1.02
f0	pUC21	10 mM methanoate + 10 mM pyruvate	0.0029±3.00E-04		
f1	[GNP] = 10 [pUC21]	10 mM methanoate + 10 mM pyruvate	0.0032±5.00E-04		1.10

[a] σ : the scavenging capacity.

[b] SSB_{XAu}/SSB_X: the ratio between the number of single strand breaks after irradiation in presence and in absence of GNP (SSB_{XAu} and SSB_X, respectively)

Table 2. Number of single strand breaks (SSB) of plasmid DNA after irradiation with ultrasoft X - rays in the absence and presence of GNP and scavengers at various concentrations. The plasmid DNA concentration is constant all over the set of experiments (see line a0 for its value). When GNPs are added, it is always at the concentration [GNP] = 10 [pUC21]. Except for the first pair of experiments (a0,a1) all other pairs of experiments (*i.e.* without and with GNPs) are performed with identical concentrations of the specific scavengers. For each line of the table, SSB constitute the slope stemming from a linear regression performed at experimental points (SSB . $plasmid^{-1}$ vs. dose); SD stands for the associated standard deviation.

This difference can be explained by noticing that TRIS and Na^+ ions shield the charge on DNA's phosphate residues to a similar extent [50], TRIS is thus probably closer to the DNA plasmids and to gold nanoparticles (in the case where they are added to plasmid DNA) than DMSO. It is actually likely that the positive charge of TRIS favors not only the electrostatic interaction with the negative charges of DNA polyanions but also with citrate gold nanoparticles. Such interaction is unlikely to be established with DMSO since it carries no electrical charge. The greatest vicinity of TRIS arising from electrostatic attraction is expected

to improve its scavenging activity since, on the one hand, it will behave as a shield and thus better protect DNA polyanion against •OH attack. On the other hand, it will block more efficiently the formation of •OH in the neighboring of the negatively-charged gold nanoparticles. The action of TRIS and DMSO can also be distinguished on the basis of the results obtained in presence of citrate-coated gold nanoparticles.

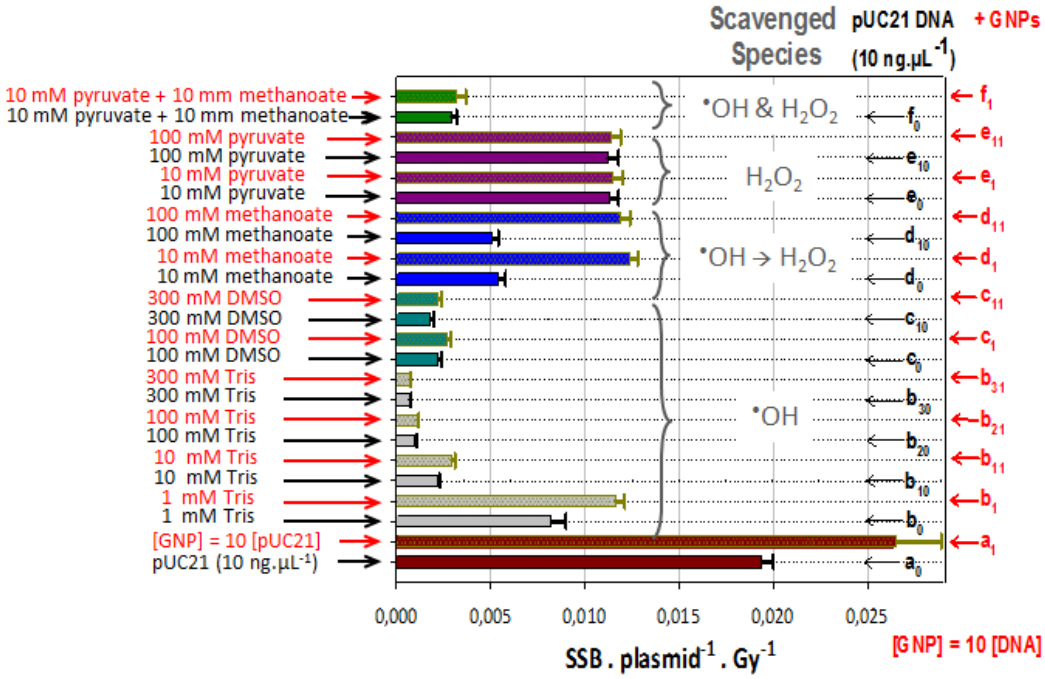

Fig. 3. *Comparison of the number of SSB per plasmid per Gray induced by ultrasoft X-ray beam in presence (1) or in absence (0) of gold nanoparticles using different scavengers. Error bars are the standard deviations for at least three measurements.*

In absence of scavengers, it appears clearly that the presence of gold nanoparticles increases the SSB yield when plasmid DNA is exposed to the ultrasoft X-ray beam since the SSB yield after irradiation in presence of gold (SSB_{XAu}) is 1.37 fold higher than the SSB number after irradiation without GNP (SSB_X), *i.e.* $SSB_{XAu}/ SSB_X = 1.37$ (Fig. 3, Table 2 lines a0 and a1). It is worth noting that in Table 2, both information about SSBs and SSB_{XAu}/SSB_X must be taken into account and compared in order to fully understand the exact consequence of each scavenger's action. The difference in SSB amount between DNA irradiated in presence or in

absence of gold nanoparticles is also observed when •OH scavengers (TRIS and DMSO) are used (Fig. 3, Table 2: comparison between b0 and b1, b10 and b11, b20 and b21, b30 and b31 for TRIS and between c0 and c1, c10 and c11 for DMSO). However in the case of TRIS, the difference attributed to the radiosensitizing effect of gold nanoparticles (R) is noticeable only at the lowest concentrations (1 and 10 mM) (Fig. 4).

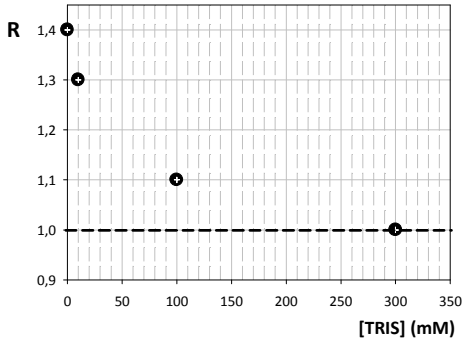

Fig. 4. *Variation of SSB_{XAu} to SSB_X ratio (R) as a function of TRIS concentration.*

Although the SSB yield decreases owing to the action of the scavenger, the efficiency of gold nanoparticles to enhance damage in DNA when TRIS is used at 1 and 10 mM remains the same than the one observed in absence of scavenger (SSB_{xAu}/SSB_x = 1.37 in absence of TRIS vs 1.41 and 1.31 in presence of TRIS (1 mM and 10 mM, respectively), Fig. 3 and Table 2: a1/a0, b1/b0 and b11/b10). In the case of higher concentration of TRIS, the effect of GNP is almost no more perceptible since SSB after irradiation in presence and in absence of GNP are nearly identical (*i.e.* SSB_{XAu}/SSB_X ~ 1, Fig. 3 and Table 2: b21/b20 and b31/b30). It can be assumed that at high concentration (100 and 300 mM) the shielding effect of TRIS is complete whereas the radiosensitizing effect of GNP, even if it is less pronounced than in absence of scavenger, is still observed at high concentration of DMSO (SSB_{XAu}/SSB_X = 1.22 at 100 and 300 mM, Fig. 3 and Table 2: c1/c0 and c11/c10). As mentioned above, the observed difference in scavenging activities of TRIS and DMSO might be understood as a consequence of the positive charge of TRIS compared to DMSO which is a neutral molecule.

Another option to limit the action of •OH consists in its conversion into hydrogen peroxide (4), this latter being considered as having no direct damaging effect on DNA in the absence of oxidizable metallic ions. For achieving this, methanoate anion was used (*vide supra*). As shown by Fig. 5 (blue curve), H_2O_2 does not generate additional SSB to plasmid DNA in absence of gold nanoparticles. The addition of methanoate in the aerated aqueous solution containing plasmid DNA limits the alteration of plasmid DNA since the SSB yields after irradiation are lower than in absence of methanoate. But the scavenging action of methanoate which is reflected by the decrease of SSB yields (in comparison to the irradiation of plasmid DNA solution without methanoate anion) is weaker than the one of TRIS or DMSO: the SSB yield after irradiation is, for a same concentration of scavengers (within the same order of magnitude of the scavenging capacity), largely higher in the presence of methanoate anion (with and without gold nanoparticles) (Fig. 3 and Table 2: d0/d11). The comparison of SSB yields after irradiation in presence or in absence of gold nanoparticles clearly indicates that •OH radicals are very aggressive species for plasmid DNA as SSB yields are very low when the action of •OH radicals is impeded by DMSO or TRIS. Moreover the action of methanoate ions does almost not depend on their concentration. The part of Fig. 3 devoted to the scavenging effect of methanoate (cases d0-d11) shows that the amount of SSB is quite the same at 10 mM and 100 mM (when comparing on the one hand the absence of gold nanoparticles and on the other hand their presence). However it must be pointed out that the presence of gold nanoparticles during irradiation results in a higher amount of SSB. The ratio of SSB number in presence and in absence of gold nanoparticles (SSB_{XAu}/SSB_X), determined for methanoate (2.29 at 10 mM and 2.33 at 100 mM), is higher than the ratio measured without scavenger (1.37) while this ratio is similar to the one of TRIS at low concentration (i.e. 1.41 at 1 mM and 1.31 at 10 mM) and it is lower than for TRIS at high concentration, DMSO, pyruvate and for the mixture (methanoate + pyruvate) (Fig. 3 and Table 2). In other

words, there is evidence that the radiosensitizing effect of gold nanoparticles is somewhat increased in presence of methanoate which paradoxically was added in order to convert $^{\bullet}OH$ into H_2O_2. There seems thus to be a peculiar interaction between citrate-coated gold nanoparticles and H_2O_2. This assertion is confirmed by the use of pyruvate which is an effective specific scavenger of H_2O_2. The addition of pyruvate led to the annihilation of the radiosensitizing effect of gold nanoparticles since the difference between SSB numbers of plasmid exposed to ultrasoft X-ray in presence or in absence of gold nanoparticles is very weak (*i.e.* SSB_{XAu}/SSB_X ~1 (Fig. 3 and Table 2: e0-e11)). Moreover the high radiosensitization efficiency of gold nanoparticles in presence of methanoate, *i.e.* in presence of H_2O_2, is seriously altered when pyruvate and methanoate are both mixed to plasmid DNA, as revealed by SSB_{XAu}/SSB_X ratio which decreases from ~2.29 to 1.10 (Table 2: d1/d0 and f1/f0). The different experiments performed on aqueous solutions of plasmid DNA with ultrasoft X-rays in presence of methanoate, pyruvate and of a mixture of (methanoate + pyruvate) highlight the role of H_2O_2 in the radiosensitizing effect of gold nanoparticles. Indeed, the enrichment of the aqueous solution of plasmid DNA with H_2O_2 (thanks to the conversion of $^{\bullet}OH$ promoted by the addition of methanoate) generates a reinforcement of the radiosensitizing effect of the gold nanoparticles whereas the radiosensitizing effect is not observed anymore when H_2O_2 is scavenged (*i.e.* when pyruvate is added). This result is very interesting since by H_2O_2 alone cannot damage plasmid DNA. As would have been anticipated, additional experiments confirm that the addition of H_2O_2 to an aqueous solution of plasmid DNA does not induce supplementary SSB in absence of gold nanoparticle and radiation (Fig. 5). But, in these additional experiments it is found that the SSB yield obviously increases when the addition of H_2O_2 is performed in presence of gold nanoparticles as revealed by the decrease of % of SC topology of the plasmid DNA (Fig. 5). We demonstrate

thus that the observed DNA damages in absence of stirring (red dashed curve) can only be due to the combined action of H_2O_2.and GNPs.

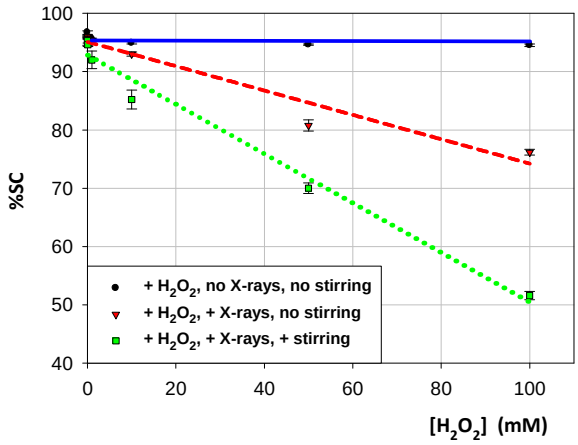

Fig. 5 *Effect of H_2O_2 on plasmid DNA in absence (blue curve) and in presence (red and green curves) of gold nanoparticles (10 nm) with (dotted green line) and without (dashed red line) stirring. Error bars stand for the standard deviations relative to at least three measurements.*

In Figure 5, the red dashed curve stands for DNA + GNPs + X-rays without stirring. In that special case, we have previously demonstrated [31] that when stirring is absent, the 1.5 keV Aluminum alpha line has extremely low penetration in liquid water. The estimate of the total penetration depth of such USX photons is indeed less than 50 µm. The height of the used 100 µL liquid samples is 2 mm; namely 40 times the estimate of the total penetration depth. In addition, during the time laps of an experiment performed at ambient temperature; $^{\bullet}OH$ radicals have an average diffusion distance largely less than 1 µm [31], that is why stirring is indispensable. Thus with the exception of the very thin irradiated layer which contributes to less than 2.5% of the total volume, the red curve accounts for an experiment in which no X-rays are absorbed in 97.5% of the samples. The effect of DNA damaging by Fenton assisted catalysis of the GNPs appears thus obviously in that special case. Lastly, experiments of Fenton assisted catalysis by GNPs in which H_2O_2 and GNPs are present without X-rays and without stirring were already performed by others [24]. The combination of H_2O_2 and citrate

gold nanoparticles thus appears as highly aggressive for plasmid DNA. The radiosensitizing effect of gold nanoparticles consists in a cleavage of H_2O_2 promoted by the gold nanoparticles. H_2O_2 can therefore be envisaged as a quiet $^{\bullet}OH$ reservoir which is activated in presence of gold nanoparticles. Although the mechanism is not elucidated herein, Fenton reactions which designate the decomposition of H_2O_2 into $^{\bullet}OH$ in presence of metallic Au(0) atoms and ions such as Au(I) (present at the surface of the gold nanoparticles) and the catalytic effect of gold nanoparticles constitute the most probable routes for explaining the deleterious action of H_2O_2 onto plasmid DNA in presence of the gold nanoparticles [23], [24]. Previous ESR experiments highlighted the role of noble metal nanoparticles (Au, Pt and Pd nanoparticles) as catalyst in the decomposition of H_2O_2 which yields $^{\bullet}OH$ radicals under acidic conditions [51], [52], [53].

IV. Conclusion

From this study based on the use of scavengers we can confirm (i) the dependence between the size of the gold core and the radiosensitizing effect (smaller is the core, greater is the radiosensitization) and (ii) the role of radicals and particularly of $^{\bullet}OH$ species. The main result of this study lies in the determination of the role of H_2O_2 which can be considered as a crucial actor of the radiosensitization. Although H_2O_2 is relatively inert toward DNA, this molecule which is in large part formed from the combination of two $^{\bullet}OH$ radicals after exposure to ionizing radiation becomes very reactive in presence of gold nanoparticles due to its catalytic decomposition into hydroxyl radical. H_2O_2 can be seen as a reservoir of $^{\bullet}OH$ radicals which are only released in presence of gold nanoparticles. At least part of the radiosensitization of the gold nanoparticles which exhibit a promising potential for improving the selectivity of radiotherapy (greater damage in the tumor and better preservation of healthy surrounding tissue) can be explained by the “activation” of the quiet $^{\bullet}OH$ reservoir that H_2O_2 molecules

constitute. Of course, the damaging effect observed here using DNA plasmids as probes can be transposed to most of biologically relevant molecules such as for example cell membranes [54], proteins, [55] etc. In this work, it was possible to experimentally demonstrate the damaging role of H_2O_2 in presence of GNP due to the very high ionization density of 1.5 keV USX in water. In other words, this was possible due to the rather small fraction of $^{\bullet}OH$ radicals surviving during the early times of water radiolysis (recombination forming hydrogen peroxide). Nevertheless, such an effect should not be neglected as it may be part of the complete set of damaging pathways associated with GNP radiosensitization in aqueous media. Lastly, as mentioned by others in the context of a recent review paper, radiosentitization of GNP can only be explained if the nanoparticle surface has specific properties as non-standard water interface organization and/or catalytic reactivity [56,57], this is precisely what was demonstrated here concerning the role of hydrogen peroxide.

Acknowledgments

This work was partially supported by a grant from the Iraqi embassy (Ph.D. of T. T. Khalil). The authors thank Farhan Bouraleh Hoch for its helpful contribution in the synthesis and characterization of GNP.

References :

[1] G. Delaney, S. Jacob, C. Featherstone and M. Barton, The role of radiotherapy in cancer treatment: Estimating optimal utilization from a review of evidence-based clinical guidelines. Cancer 104 (2005) 1129.

[2] K.M. Prise, Ionizing Radiation Therapy. In: Schwab M. (eds) Encyclopedia of Cancer. 2011. Springer, Berlin, Heidelberg

[3] K. Kobayashi, N. Usami, E. Porcel, S. Lacombe and C. Le Sech, Enhancement of radiation effect by heavy elements. Mutat. Res. -Rev. Mutat. Res. 704 (2010) 123.

[4] E. Bräuer-Krisch, R. E. Serduc, A. Siegbahn, G. Le Duc, Y. Prezado, A. Bravin, H. Blattmann and J. A. Laissue, Effects of pulsed, spatially fractionated, microscopic synchrotron X-ray beams on normal and tumoral brain tissue. Mutat. Res. -Rev. Mutat. Res. 704 (2010) 160.

[5] D. A. Scheinberg, C. H. Villa, F. E. Escorcia and M. R. McDevitt, Conscripts of the infinite armada: Systemic cancer therapy using nanomaterials. Nat. Rev. Clin. Oncol. 7 (2010) 266.

[6] N. Bertrand and J.C. Leroux, The journey of a drug-carrier in the body: An anatomo-physiological perspective. J. Control. Release 161 (2012) 152.

[7] M. Yu, and J. Zheng, Clearance Pathways and Tumor Targeting of Imaging Nanoparticles. ACS Nano, 9 (2015) 6655.

[8] D.E. Lee, H. Koo, I.C. Sun, J. H. Ryu, K. Kim and I. C. Kwon, Multifunctional nanoparticles for multimodal imaging and theragnosis. Chem. Soc. Rev. 41 (2012) 2656.

[9] S. Kunjachan, J. Ehling, G. Storm, F. Kiessling and T. Lammers, Noninvasive imaging of nanomedicines and nanotheranostics: Principles, progress, and prospects. Chem. Res. 115 (2015) 10907.

[10] C. Alric, R. Bazzi, F. Lux, G. Laurent, M. Martini, M. Dutreix, G. Le Duc, P. Perriat, S. Roux and O. Tillement, The design of hybrid nanoparticles for image-guided radiotherapy. In Functional Nanoparticles for Bioanalysis, Nanomedicine, and Bioelectronic Devices 2 (2012)95.

[11] I. Miladi, C. Alric, S. Dufort, P. Mowat, A. Dutour, C. Mandon, G. Laurent, E. Bräuer-Krisch, N. Herath, J.-L. Coll, M. Dutreix, F. Lux, R. Bazzi, C. Billotey, M. Janier, P. Perriat, G. Le Duc, S. Roux, O. Tillement, The in vivo radiosensitizing effect of gold nanoparticles based MRI contrast agents. Small 10 (2014) 1116.

[12] G. Le Duc, I. Miladi, C. Alric, P. Mowat, E. Bräuer-Krisch, A. Bouchet, E. Khalil, C. Billotey , M.Janier, F. Lux , T. Epicier, P. Perriat, S. Roux, and O. Tilement et al., Toward an image-guided microbeam radiation therapy using gadolinium-based nanoparticles. ACS Nano 5 (2011) 9566.

[13] X. Liu, X. Zhang, M. Zhu, G. Lin, J. Liu, Z. Zhou, X. Tian, Y. Pan, PEGylated Au@Pt nanodendrites as novel theranostic agents for computed tomography imaging and photothermal/radiation synergistic therapy. ACS Appl. Mater. Interfaces 9 (2017) 279.

[14] D. M. Herold, I. J. Das, C. C. Stobbe, R. V. Iyer and J. D. Chapman, Gold microspheres: a selective technique for producing biologically effective dose enhancement. Int. J. Radiat. Biol. 76 (2000) 1357.

[15] J. F. Hainfeld, D. N. Slatkin and H. M. Smilowitz, The use of gold nanoparticles to enhance radiotherapy in mice. Phys. Med. Biol. 49 (2004) 309.

[16] C. Alric, I. Miladi, D. Kryza, J. Taleb, F. Lux, R. Bazzi, C. Billotey, M. Janier, P. Perriat, S. Roux, O. Tillement, The biodistribution of gold nanoparticles designed for renal clearance. Nanoscale 5 (2013) 5930.

[17] K. T.Butterworth, J. A. Coulter, S. Jain, J. Forker, S. J. McMahon, G. Schettino, K. M. Prise, F. J. Currell and D. G. Hirst, Evaluation of cytotoxicity and radiation enhancement using 1.9 nm gold particles: Potential application for cancer therapy. Nanotechnology 21 (2010) 295101.

[18] S. J. McMahon, W. B. Hyland, M. F. Muir, J. A. Coulter, S. Jain, K. T. Butteworth, G.Schettino, G. R. Dickson, A. R. Hounsell, J. M. O'Sullivan, K.M. Prise, D. G. Hirst, F. J. Curell, Biological consequences of nanoscale energy deposition near irradiated heavy atom nanoparticles. Sci. Rep. 1 (2011) 18.

[19] K. T. Butterworth, S. J. McMahon, F. J. Currell and K.M. Prise, Physical basis and biological mechanisms of gold nanoparticle radiosensitization. Nanoscale 4 (2012) 4830.

[20] M. Misawa and J. Takahashi, Generation of reactive oxygen species induced by gold nanoparticles under X-ray and UV irradiations. Nanomedicine 7 (2011) 604.

[21] C. Sicard-Roselli, E. Brun, M. Gilles, G. Baldacchino, C. Kelsey, H. McQuaid, C. Polin, N. Wardlow and F. A; Currel, New mechanism for hydroxyl radical production in irradiated nanoparticle solutions. Small 10 (2014) 3338.

[22] K. Haume, S. Rosa, S. Grellet, M. A. Śmiałek, K. T. Butterworth, A. V. Solov'yov, K. M. Prise, J. Golding and N. J. Mason. Gold nanoparticles for cancer radiotherapy: a review. Cancer Nano 7:8 (2016).

[23] A. Thetford, G. J. Hutchings, S. H. Taylor, D. J. Willock. The decomposition of H_2O_2 over the components of Au/TiO_2 catalysts. Proc. R. Soc. A 467 (2011), 1885.

[24] S. Navalon, R. Martin, M. Alvaro, H. Garcia. Gold on diamond nanoparticles as a highly efficient Fenton catalyst. Angew. Chem. Int. Ed. 49 (2010) 8403.

[25] Fulford, J. Bonner, P. Goodhead, D.T. Hill, M.A. O'Neill, P. Experimental determination of the dependence of OH radical yield on photon energy: A comparison with theoretical simulation. J. Phys. Chem. A 103 (1999) 11345.

[26] J. Meesungnoen, A. Filali-Mouhim, S. Mankhetkorn, and J-P Jay-Gerin. Comment on "Experimental Determination of the Dependence of OH Radical Yield on Photon Energy: A Comparison with Theoretical Simulations" by Fulford et al. (J. Phys. Chem. A 1999, 103, 11345−11349). J. Phys. Chem. A 105 (2001)2125.

[27] R. Watanabe and K. Saito. Monte Carlo simulation of strand-break induction on plasmid DNA in aqueous solution by monoenergetic electrons. Radiat Environ Biophys 41 (2002) 207.

[28] J. A. Imlay, S. M. Chin, S. Linn. Toxic DNA damage by hydrogen peroxide through the Fenton reaction in vivo and in vitro. Science 240 (1988) 640.

[29] K.L. Manchester, When are nucleic acids not nucleic acids? Problems with estimation of nucleic acid purity by UV absorbance. Biochem. Educ. 25 (1997) 214.

[30] G. Frens, Controlled nucleation for the regulation of the particle size in monodisperse gold suspensions. Nature 241 (1973) 20.

[31] M. Souici, T.T. Khalil, O. Boulanouar, A. Belafrites, C. Mavon, M. Fromm, DNA strand break dependence on Tris and arginine scavenger concentrations under ultra-soft X-ray irradiation: the contribution of secondary arginine radicals. Radiat. Environ. Biophys. 55 (2016) 215.

[32] R. Cowan, C.M. Collis and G.W. Grigg, Breakage of double-stranded DNA due to single-stranded nicking. J. Theor. Biol. 127 (1987) 229.

[33] M. Brust, M. Walker, D. Bethell, D. J. Schiffrin, R. Whyman, Synthesis of thiol-derivatized gold nanoparticles in a 2-phase liquid-liquid system. J. Chem. Soc. Chem. Commun. 7 (1994) 801.

[34] S. K. Ghosh, T. Pal, Interparticle coupling effect on the surface plasmon resonance of gold nanoparticles: from theory to applications. Chem. Rev. 107 (2007) 4797.

[35] H. Yamaguchi, Y. Uchihori, N. Yasuda, M. Takada, H. Kitamura, Estimation of yields of OH radicals in water irradiated by ionizing radiation. J. Radiat. Res. 46 (2005) 333.

[36] M. J. Burkitt and R. P. Mason, Direct evidence for in vivo hydroxyl-radical generation in experimental iron overload: an ESR spin-trapping investigation. Proc. Natl Acad. Sci. USA 88 (1991) 8440.

[37] M. Hicks and J. M. Gebicki, Rate constants for reaction of hydroxyl radicals with Tris, Tricine and Hepes buffers. FEBS Lett. 199 (1986) 92.

[38] D. Veltwisch, E. Janata; K.D. Asmus, Primary processes in the reactions of •OH radicals with sulfoxides. J. Chem. Soc., Perkin Trans. 2 (1980) 146.

[39] R.L. Willson, C.L. Greenstock, G.E. Adams, R. Wageman, L.M. Dorfman, The standardization of hydroxyl radical rate data from radiation chemistry. Int. J. Radiat. Phys. Chem. 3 (1971) 211.

[40] J. Meesungnoen and J. Jay-Gerin Effect of multiple ionization on the yield of H_2O_2 produced in the radiolysis of aqueous 0.4 M H_2SO_4 solutions by high-LET $12C^{6+}$ and $20Ne^{9+}$ ions. Radiat. Res. 164 (2005) 688.

[41] B.H.J. Bielski, D.E. Cabelli, R.L. Arudi and A.B. Ross, Reactivity of $HO_2/O_2^{\bullet-}$ radicals in aqueous solution. J. Phys. Chem. Ref. Data 14 (1985) 1041.

[42] R. Roots and S. Okada, Estimation of life times and diffusion distances of radicals involved in X-Ray-induced DNA strand breaks or killing of mammalian cells. Radiat. Res. 64 (1975) 306.

[43] A. Kupperman, Diffusion model of the radiation chemistry of aqueous solutions. In Silini G (ed) Radiation Research. North-Holland Publishing Co. Amsterdam (1967) 212.

[44] L. Schöne and H. Herrmann, Kinetic measurements of the reactivity of hydrogen peroxide and ozone towards small atmospherically relevant aldehydes, ketones and organic acids in aqueous solutions. Atmos. Chem. Phys. 14 (2014) 4503.

[45] J. Lee, N. Koo and D.B. Min, Reactive oxygen species, aging, and antioxidative nutraceuticals. Comprehensive Reviews in Food Science and Food Safety – CRFSFS 3 (2004) 21.

[46] D. A. Hems and J. T. Brosnan, Effect of ischaemia on content of metabolites in rat liver and kidney in vivo. Biochem. J. 120 (1970) 105.

[47] T. Y. Aw, B. S. Andersson and D. P. Jones, Mitochondrial transmembrane ion distribution during anoxia. Am. J. Physiol. 252 (Cell Physiol. 21) (1987) C356.

[48] M.M. Bayliak, M.P. Lylyk, O.M. Vytvytska, V. I. Lushchak, Assessment of antioxidant properties of alpha‑keto acids in vitro and in vivo. Eur Food Res Technol 242 (2016) 179.

[49] J. Vásquez-Vivar, A. Denicola, R. Radi and O. Augusto, Peroxynitrite-mediated decarboxylation of pyruvate to both carbon dioxide and carbon dioxide radical anion. Chem. Res. Toxicol. 7 (1997) 786.

[50] N. C. Stellwagen, A. Bossi, C. Gelfi, and P. G. Righetti. DNA and buffers: Are there any noninteracting, neutral pH buffers? Analytical Biochemistry 287 (2000) 167.

[51] W. He, Y. T. Zhou, W. G. Wamer, X. Hu, X. Wu, Z. Zheng, M. D. Boudreau, J. J. Yin, Intrinsic catalytic activity of Au nanoparticles with respect to hydrogen peroxide decomposition and superoxide scavenging. Biomaterials 34 (2013) 765.

[52] Y. Liu, H. Wu, M. Li, J.-J. Yin, Z. Nie, pH dependent catalytic activities of platinum nanoparticles with respect to the decomposition of hydrogen peroxide and scavenging of superoxide and singlet oxygen. Nanoscale 6 (2014) 11904.

[53] T. Wen, W. He, Y. Chong, Y. Liu, J.-J. Yin, X. Wu, Exploring environment-dependent effects of Pd nanostructures on reactive oxygen species (ROS) using electron spin resonance (ESR) technique: implications for biomedical applications. Phys.Chem.Chem.Phys. 17 (2015) 24937.

[54] R. T. Dean. Free radicals, membrane damage and cell-mediated cytolysis. N. C.Br J. Cancer Suppl. 8 (1987) 39.

[55] R. T. Dean, S. Fu, R. Stocker and M. J. Davies. Biochemistry and pathology of radical- mediated protein oxidation. Biochem. J. 324 (1997) 1.

[56] E. Brun, C. Sicard-Roselli. Actual questions raised by nanoparticle radiosensitization. Radiation Physics and Chemistry 128 (2016) 134–142.

[57] M. Gilles, E. Brun and C. Sicard-Roselli, Quantification of hydroxyl radicals and solvated electrons produced by irradiated gold nanoparticles suggests a crucial role of interfacial water. Journal of Colloid and Interface Science 525, 2018, 31-38.